ELSEVIER

Journal of Nuclear Materials 266–269 (1999) 296–301

journal of nuclear materials

Operational performance of JT-60U W-shaped divertor

N. Hosogane [a,*], H. Tamai [a], S. Higashijima [a], H. Kubo [a], A. Sakasai [a], H. Takenaga [a], K. Itami [a], S. Sakurai [a], N. Asakura [a], S. Konoshima [a], T. Sugie [a], K. Shimizu [a], T. Ishijima [b], A. Kumagai [b], S. Suzuki [a], M. Shimada [a]

[a] *Japan Atomic Energy Research Institute, Naka Fusion Research Establishment, Naka-machi, Naka-gun, Ibaraki-ken 311-01, Japan*
[b] *University of Tsukuba, 1-1-1 Tenoudai, Tsukuba-shi, Ibaraki-ken 305, Japan*

Abstract

Performance of inner leg pumping of JT-60U W-shaped divertor is presented. Inner leg pumping works well as the dome separates inner and outer divertor channels for neutral particles in the private flux region. In ELMy H-mode with NBI heating power of 18 MW, the operational regime where inner leg pumping is effective extends to the divertor radiation range of about 60% of SOL power. The fraction of inner particle flux pumped is estimated to be about 3%. It is qualitatively shown that a combination of main gas puff and inner leg pumping reduces carbon impurities in the main plasma, suggesting the existence of SOL flow effect on impurity reduction. © 1999 Elsevier Science B.V. All rights reserved.

Keywords: JT-60U; Divertor asymmetry; Divertor pumping; Impurity reduction

1. Introduction

Divertor pumping is an essential tool for plasma density control, helium ash exhaust, SOL flow formation and radiative divertor control. To obtain good performance of divertor pumping, the pumping location should be optimized. For example, according to simulation results, it may be difficult to exhaust helium ash from the private flux region for attached plasma [1]. SOL flow formation for impurity reduction will require large pumping capability [2,3]. In the present design of ITER, divertor pumping from the private flux region is now planned. However, the effects of pumping location on these control issues as well as divertor characteristics have not been clarified yet. Therefore, in present tokamaks, pumping from both leg channels in the private flux region [4,5] like ITER or from the public region at the outer leg channel [2,3] have been studied. Comparison of operational performance among tokamaks with different pumping schemes is important for understanding effects of pumping on divertor characteristics, and will yield an important database for designing the next tokamaks like ITER.

In JT-60U, the previous open divertor was modified to a W-shaped divertor with pumps from February to May in 1997 [6]. As a pumping scheme for the W-shaped divertor, inner leg pumping (i e., pumping from the inner divertor channel) in the private flux region was adopted on the first step for experiments in 1997, and pumping from both legs was planned on the second step for comparison of divertor pumping performance. The inner pumping scheme takes advantage of strong in–out asymmetry of particle recycling [7]. Since the neutral pressure in the inner divertor channel becomes larger than the outer one, it is possible to get the same throughput with small pumping speed in the inner pumping scheme compared with the outer pumping scheme. This is a special feature for the W-shaped divertor which has not been found in other divertors.

This paper presents operational performance of the W-shaped divertor related with inner leg pumping. In Section 2, the pumping system of the W-shaped divertor is explained. In Section 3, in–out asymmetric characteristics of divertor particle flux are clarified. In Sec-

* Corresponding author. Tel.: +81-29 270 7341; fax: +81-29 270 7449; e-mail: hosogane@naka.jaeri.go.jp

0022-3115/99/$ – see front matter
PII: S0022-3115(98)00820-4

tion 4, pumping capability of the W-shaped divertor is discussed. In Section 5, the effect of gas puff and pumping on reduction of carbon impurities is presented. A summary is given in Section 6.

2. Pumping system of W-shaped divertor

A cross-section view of the W-shaped divertor [6] is shown in Fig. 1. The divertor consists of inclined divertor plates and a dome arranged in a W-shaped configuration, as well as inner baffles and outer baffles for a pumping duct. The dome is expected to separate inner and outer leg sides geometrically for particle recycling. Divertor pumping is done from inner leg side in the private flux region, i.e., inner leg pumping. The pumping slot of 3 cm width is arranged between the inner divertor plates and the inner wing of the dome continuously in the toroidal direction. The gap between the outer divertor plates and the outer wing of the dome is closed with thin plates behind tiles. Three pumping ports (ϕ 0.6 m $\times$ 4.8 m) are connected to the duct under the baffle. They are arranged at three port sections, P-4, P12 and P-16. The toroidal uniformity of the neutral pressure in the duct due to the port arrangement is estimated to be within ±20%. Cryopumps with pumping speed of 1000 m^3/s each are used for divertor pumping. The measured net pumping speed at the pumping slot in the divertor region is 13 m^3/s in molecular flow. The reduction in pumping speed is mainly attributed to conductance of pumping ports and narrow gaps from the dome to the outer divertor. However, a large capacity of cryopump can afford a steady pumping state even when a large gas puff is applied continuously. Gas fueling valves are installed at the top of vacuum vessel for main gas puff (three ports) and in the divertor region for divertor gas puff (two ports).

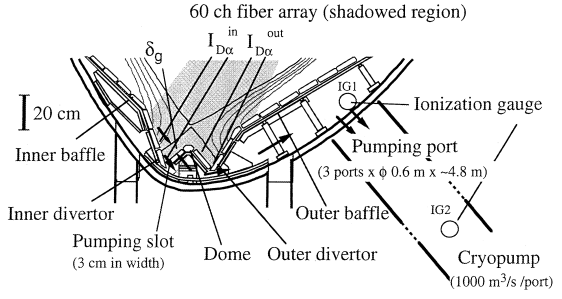

Fig. 1. Cross sectional structure of W-shaped divertor. δ_g is a gap between the inner leg and the dome wing. Ionization gauge IG1 is arranged at a short port (0.5 m) in the P-18 section and IG2 at about 0.8 m from the exit of the pumping port in the P-4 section.

3. Operational regime with in–out asymmetric particle recycling in the divertor

Fig. 2 shows divertor radiation loss fraction of SOL power ($= P_{heat} - P_{rad}^{main}$) and D_α intensities at the inner and outer divertor (Fig. 1) obtained in ELMy H-mode discharges as a function of main electron density. Three series of ELMy H-modes are used in this plot: (1) normal B_T and main/divertor gas puff ($I_p = 1.2$ MA, $B_T = 2.5$ T, $P_{NBI} = 18$ MW), (2) normal B_T and no gas puff ($I_p = 1.5$ MA, $B_T = 3.6$ T, $P_{NBI} = 22$–25 MW, long pulse up to 9 s) and (3) reversed B_T and main gas puff ($I_p = 1.4$–1.7 MA, $B_T = 35$ T, $P_{NBI} = 12$ MW). The divertor radiation loss fraction is plotted using data from (1) which covers the wide density regime before and after the onset of X-point MARFE. The inner and outer D_α intensities show the relative behavior of particle fluxes to the inner and outer divertors, provided that the number of ionization events per D_α photon is not sensitive to the variation of divertor states. This condition is considered to hold in the discharges discussed here as explained later in this section.

The inner particle flux, shown by the inner D_α intensity, increases with main electron density in a nonlinear manner much stronger than the outer one before the onset of X-point MARFE, leading to the formation of strong in–out asymmetry of particle recycling. According to Langmuir probe measurements, the large

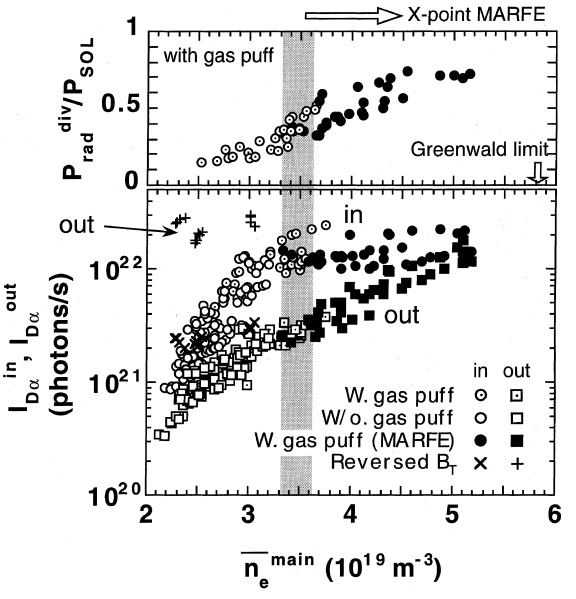

Fig. 2. Inner and outer D_α intensity and divertor radiation fraction as a function of electron density. X-point MARFE are shown by closed symbols. Normal ion grad_B drift direction is toward the divertor. Divertor radiation losses are plotted using the data in 1.2 MA discharges with gas puff.

increase in inner particle flux is triggered by detachment of inner divertor plasma (i.e., beginning of the decrease in ion saturation current). The X-point MARFE occurs when the outer separatrix becomes detached. After the onset of X-point MARFE, the inner particle flux becomes saturated or decreases.

While, as the outer particle flux continues to increase with electron density, the in–out asymmetry of particle flux becomes reduced or reversed (see Fig. 3 for L-mode case or Ref. [8]). The similar trend has been observed in JET [9]. The X-point MARFE occurs around radiation loss fraction of 35% of SOL power. Before the onset of X-point MARFE, similarly to the behavior of the particle flux, the divertor radiation loss increases with in–out asymmetric profiles with large inner side. After the onset of X-point MARFE, corresponding to the saturation or reduction of the inner particle flux, the radiation loss at the inner divertor side does not increase. In contrast to the inner divertor side, the radiation loss around the X-point increases with the increase in outer particle flux and exceeds both side radiation losses as the radiation loss fraction reaches around 60% of SOL power. The similar behavior of radiation loss was observed in the previous open divertor [10].

In these plots, it is noted that the inner particle flux is still larger than the outer particle flux until the electron density approaches to the Greenwald limit of 1.2 MA discharges shown by arrow. The divertor radiation loss in this regime is extrapolated to about 80% of SOL power. This suggests that pumping from the higher recycling side, i.e., inner leg pumping, will be effective even in the X-point MARFE regime. However, for controlling the radiative divertor state accompanied by a strong X-point MARFE with large radiation loss fraction, for example, more than 60%, the effect of outer leg pumping should also be taken into consideration.

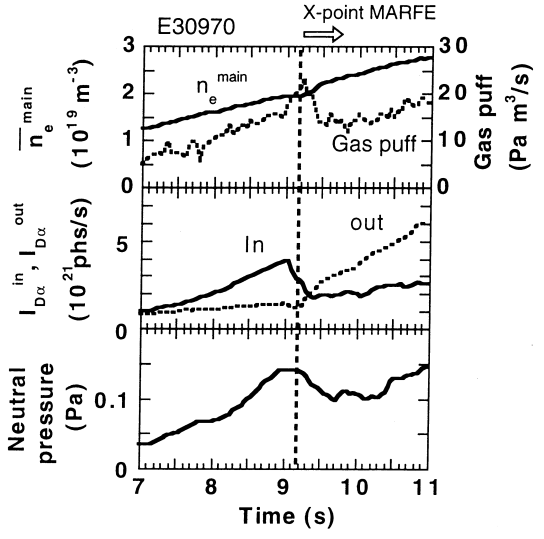

Fig. 3. Time evolution of an L-mode discharge with turnover of inner and outer D_α intensity before and after onset of X-point MARFE.

The operational regime discussed here covers from attached divertor ($n_e^{main} < 2.5 \times 10^{19}$ m^{-3} for the inner side) to detached divertor with X-point MARFE, and variation of electron temperature and density, in general, has influence on the estimation of particle flux from D_α line intensity. However, in detached divertor states in JT-60U, unlike Alcator C-Mod [11] or JET [12], the volume recombination process is not predominant and the ratio of recombination sink to ionization source is small (1–3%) [13]. The D_α line radiation comes mainly from the region with higher electron temperature, where the recycling particles are ionized (ionization front) [7]. Consequently, the ionization event number per D_α photon to be used to estimate particle flux is considered to weakly depend on the divertor states.

4. Inner leg pumping characteristics

In the W-shaped divertor, the dome is expected to play a role of separating the inner and outer leg region for motion of neutral particles. To confirm such a geometrical effect of the dome, a relationship between particle flux to the divertor region estimated by D_α intensity and neutral particle pressure in the duct has been investigated.

Fig. 3 shows the time evolution of inner and outer D_α intensities and neutral pressure in the duct under the baffle (IG1 in Fig. 1) in an L-mode discharge with $I_p = 1.2$ MA, $B_T = 3.5$ T (normal B_T) and $P_{NBI} = 4$ MW. X-point MARFE occurred at 9.2 s in this discharge. A remarkable turnover of the inner and outer D_α intensities is seen before and after the onset of an X-point MARFE. Turnover like this has been observed when an X-point MARFE grows [8]. Here, it is noted that even with such a turnover, the neutral pressure in the duct almost follows the change in inner D_α intensity before and after the onset of the X-point MARFE. This means that the inner and outer divertor channels are well separated for behavior of neutral particles by the dome. This is confirmed by experimental results that relationships of neutral particle pressure in the duct under the baffle and in the pumping port with the inner D_α intensity are almost linear as shown in Fig. 4. In this figure, data are plotted using the same discharges as Fig. 2. Furthermore, even in discharges with reversed B_T, where the in–out asymmetry of particle recycling is reversed as shown in Fig. 2, the port pressure is found to be determined by the inner particle flux. These results show that inner leg pumping works well.

From the relationship of the neutral pressure in the duct under the baffle with the D_α intensity shown in

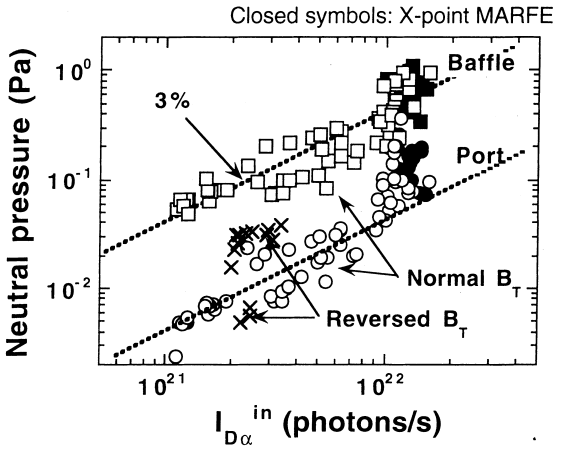

Fig. 4. Neutral pressure in the duct under the baffle (baffle) and in the port (port) as a function of inner D_α intensity. Linear relationships show that inner leg pumping worked well. As for discharges with reversed B_T, only port pressure was measured.

Fig. 4, pumping efficiency of the inner pumping, which is defined by the ratio of the throughput to the inner particle flux, is estimated. The effective conductance from the duct with the ionization gauge IG 1 to the cryopump is estimated to be 60–80 m^3/s at 300°C in the range of intermediate flow. With this conductance, assuming that the number of ionization events per D_α photon is 15, the ratio of throughput to inner particle flux is estimated to be about 3% as shown in Fig. 4.

5. Effect of gas puff and pump on carbon impurities

A combination of main gas puff and pump is considered to generate SOL flow necessary for impurity reduction. To obtain a sufficient SOL flow effect, pumping efficiency should be large enough to balance with the gas puff. From this viewpoint, inner leg pumping is expected to have a potential of impurity reduction.

Fig. 5 shows the time evolution of three ELMy H-mode discharges with main gas puff and pump (A, B) and with main gas puff and no pump (C) on behavior of carbon impurities. Experimental conditions are $I_p = 1.2$ MA, $B_T = 2.5$ T and $P_{NBI} = 18$ MW. H-factors of these discharges, which decrease with the increase in electron density, are 1.1–1. 2 at $n_e^{main} \sim 3.5 \times 10^{19}$ m^{-3} discussed here. ELM activity is type I and ELM frequency is 130–140 Hz before the onset of X-point MARFE and increases to 220–240 Hz with some irregular oscillations after the onset of X-point MARFE. Electron density is increased by feedback control. The difference in gas puff rate is mainly attributed to the difference in operation of pump and/or gap between inner separatrix and the pumping slot, δ_g (Fig. 1). The gap δ_g is 2 cm for the discharge A and 6 cm for the discharges B and C. The gas puff rate in the discharge with gap of 2 cm (A) is largest at the same electron density. In contrast, a small amount of gas puff is enough to increase the electron density in the discharge without pump (C), and the neutral pressure in the duct under the baffle (IGI) rises up to higher than 1 Pa. CII intensity in the divertor, as an indicator for carbon impurity generation at the divertor, was measured by a 60-channel fiber array (Fig. 1). The inner CII intensities are almost constant after the initial increase at the step-up of the NBI power. This is presumably because the inner divertor side becomes detached early as explained in Section 3. On the

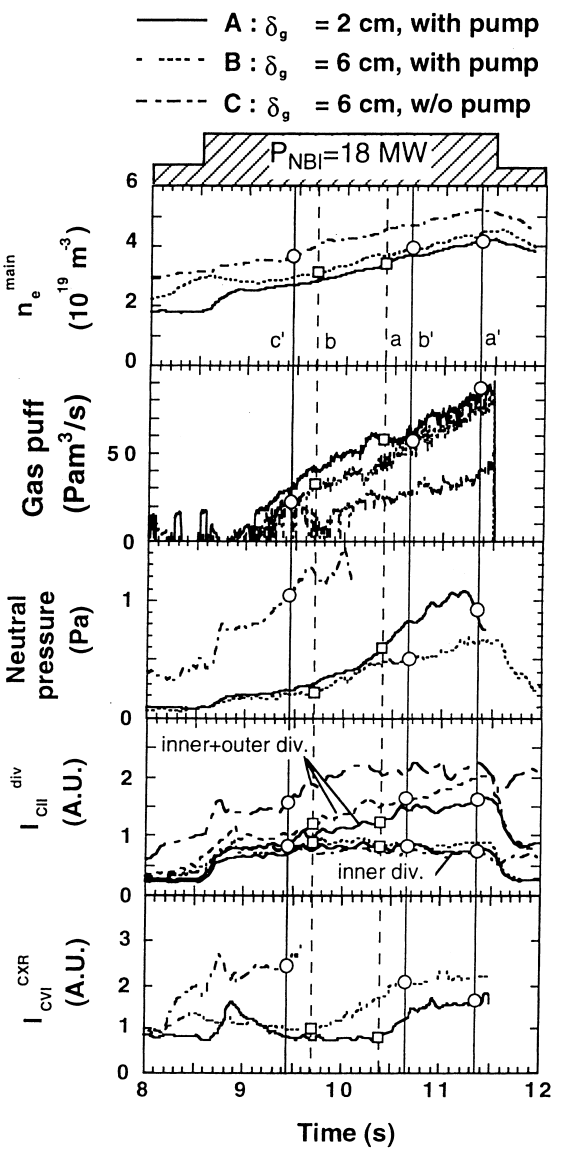

Fig. 5. Time evolution of ELMy H-mode discharges with main gas puff and pump and with main gas puff and no pump.

other hand, the outer CII intensities, shown by the difference of the total and the inner intensities, are much smaller than the inner ones meanwhile after the step-up of NBI power, and start to increase after some delay, respectively. These increases are induced by the start of X-point MARFE which is identified as a small increase of CII intensity near the X-point. Correspondingly, CVI intensities at $\rho/a = 0.6$ in the main plasma, which were measured by charge exchange recombination spectroscopy, are observed to increase. It is noted that the CVI intensity is lower in the discharge with the larger gas puff rate. This suggests the existence of SOL flow effect generated by gas puff.

Effects of the gas puff on the carbon impurity reduction should be compared between discharge states with almost the same level of carbon impurity generation in the divertor. For comparison, two sets of time of interest are picked up in Fig. 5; a and b for case (I) and a′, b′ and c′ for case (II). Case (I) is the state just before the onset of X-point MARFE in the discharges (A) and (B), while case (II) is the state during the X-point MARFE in the discharges (A), (B) and (C). Profiles of CII intensity in the divertor for cases (I) and (II) are shown in Fig. 6 (I) and (II), respectively. Taking into account the shifts of the inner peak due to the difference in gap δ_g, generation of carbon impurities in the divertor estimated from CII intensity is considered to be nearly at the same level for each case.

Relationships of electron density, particle recycling in the divertor, neutral pressure in the duct, CII intensities in the divertor as an indicator of carbon impurity source and Z_{eff} with gas puff rate are summarized in Fig. 7 for cases (I) and (II). As indicated by the strong in–out asymmetry of D_α intensity, it is noted that the particle recycling for these discharges is in the regime where the inner pumping is effective (Fig. 2). The increase in neutral pressure in the discharges with pump (A, B) indicates that the throughput of the inner pumping increases with the gas puff rate. D_α intensities in the inner divertor and the main plasma (not shown) are nearly same among the states to be compared, for example, a′, b′ and c′. Hence, the ratios of the SOL flow generated by the gas puff to the particle fluxes in the divertor and the main plasma are proportional to the gas puff rate, and reach about 0.2 and 0.8 in the state a′ with a gas puff rate of 83 Pa m^3/s. Thus, the SOL flow effect on the impurity reduction is expected as the gas puff increases. Actually, Z_{eff} is found to decrease with the increase in gas puff for

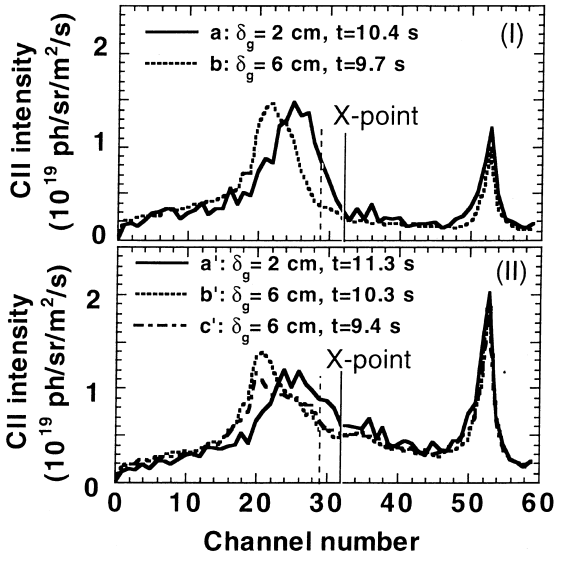

Fig. 6. Profiles of CII intensity for cases (I) and (II). Case (I): just before the onset of X-point MARFE; Case (II): during the X-point MARFE before the growth.

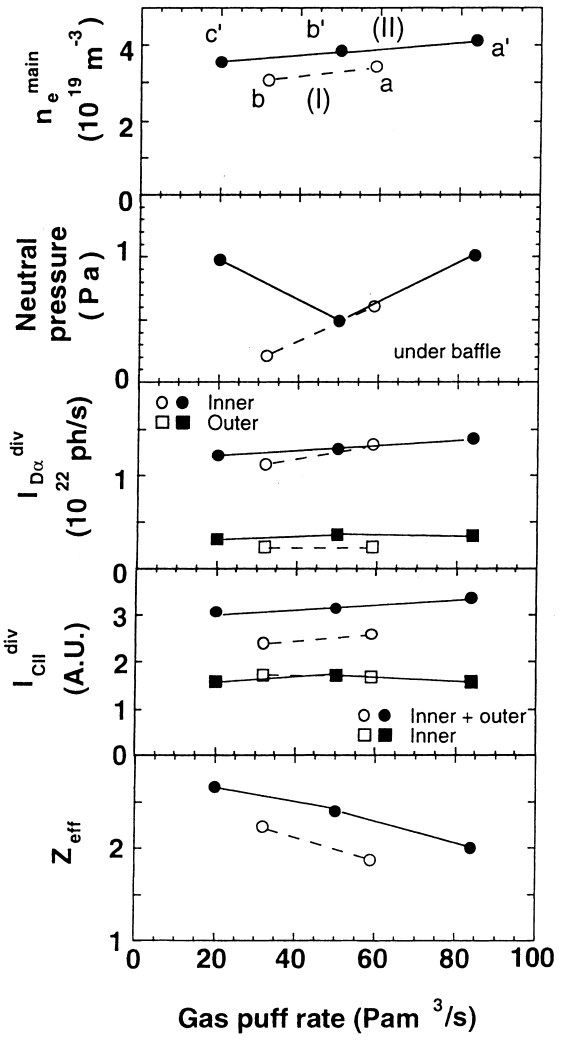

Fig. 7. Relationships of particle recycling and carbon impurity with main gas puff rate for cases (I) and (II).

both cases (I) and (II). This decrease is considered to be larger than that caused by the density increase. For example, the fraction of the decrease in Z_{eff} due to the density increase from c′ to a′ is about 40%, using a simple formula of $Z_{\text{eff}} - 1 = (Z_i^2 - Z_j) \times n_c/n_e$ on the assumption that the carbon concentration is proportional to the total CII intensity in the divertor. This result qualitatively suggests that the SOL flow is generated by the gas puff and is effective in carbon impurity reduction. It should be noted that the SOL flow effect can be obtained in the operation with inner leg pumping. With outer leg pumping only, pumping is so small in the experimental regime examined here that significant SOL flow effect may not be observed.

6. Summary

It has been experimentally confirmed that the dome separates inner and outer divertor channels for neutral particles, and makes it possible to pump from the inner leg channel (inner leg pumping). According to the particle recycling characteristics obtained in ELMy H-mode with NBI heating power of 18 MW, inner leg pumping is considered to be advantageous over outer leg pumping only as long as divertor radiation loss is controlled below around 60%, irrespective of attached divertor or detached divertor with X-point MARFE. The actual fraction of inner particle flux pumped was about 3%. It has been shown that a combination of main gas puff and inner leg pumping reduces carbon impurities in the main plasma in ELMy H-mode.

Acknowledgements

The author would like to thank the members of the Japan Atomic Energy Research Institute who have contributed to the JT-60U project.

References

[1] A. Kukushkin et al., Proceedings of the 16th Fusion Energy Conference, Montreal, vol. 2, International Atomic Energy Agency, Vienna, 1996, p. 987.
[2] M.J. Schaffer et al., J. Nucl. Mater. 241–243 (1997) 585.
[3] H.-S. Bosch et al., J. Nucl. Mater. 241–243 (1997) 82.
[4] JET Team (presented by G.C. Vlases), Proceedings of the 16th Fusion Energy Conference, Montreal, vol. 1, International Atomic Energy Agency, Vienna, 1996, p. 371.
[5] R. Schneider et al., these Proceedings.
[6] N. Hosogane et al., Proceedings of the 16th Fusion Energy Conference, Montreal, vol. 3, International Atomic Energy Agency, Vienna, 1996, p. 555.
[7] N. Asakura et al., Proceedings of the 15th International Conference Plasma Physics and Controlled Nuclear Fusion Research, Seville, vol. 1, International Atomic Energy Agency, Vienna, 1994, p. 555.
[8] H. Tamai et al., Plasma Phys. Controlled Fus, submitted.
[9] A. Loarte et al., Nucl. Fusion 38 (1998) 331.
[10] N. Hosogane et al., J. Nucl. Mater. 220–222 (1995) 420.
[11] J.L. Terry et al., these Proceedings.
[12] G.M. McCracken et al., these Proceedings.
[13] H. Kubo et al., in: International Congress on Plasma Physics combined with the 25th EPS Conference on Controlled Fusion and Plasma Phys., Prague, 1998, Part I, p. 56.